Going Beyond Silver in Ethylene Epoxidation with First-Principles Catalyst Screening

How to cite: Angew. Chem. Int. Ed. 2023, e202305804
doi.org/10.1002/anie.202305804

Heterogeneous Catalysis | Hot Paper

Going Beyond Silver in Ethylene Epoxidation with First-Principles Catalyst Screening

Matej Huš, Miha Grilc, Janvit Teržan, Sašo Gyergyek, Blaž Likozar, and Anders Hellman**

Abstract: Ethylene epoxidation is industrially and commercially one of the most important selective oxidations. Silver catalysts have been state-of-the-art for decades, their efficiency steadily improving with empirical discoveries of dopants and co-catalysts. Herein, we perform a computational screening of the metals in the periodic table, identify prospective superior catalysts and experimentally demonstrate that Ag/CuPb, Ag/CuCd and Ag/CuTl outperform the pure-Ag catalysts, while they still confer an easily scalable synthesis protocol. Furthermore, we show that to harness the potential of computationally-led discovery of catalysts fully, it is essential to include the relevant in situ conditions e.g., surface oxidation, parasitic side reactions and ethylene epoxide decomposition, as neglecting such effects leads to erroneous predictions. We combine ab initio calculations, scaling relations, and rigorous reactor microkinetic modelling, which goes beyond conventional simplified steady-state or rate-determining modelling on immutable catalyst surfaces. The modelling insights have enabled us to both synthesise novel catalysts and theoretically understand experimental findings, thus, bridging the gap between first-principles simulations and industrial applications. We show that the computational catalyst design can be easily extended to include larger reaction networks and other effects, such as surface oxidations. The feasibility was confirmed by experimental agreement.

Introduction

The production of ethylene epoxide (EO) ranks among the most important catalytic reactions concerning the market value and amount of chemicals produced. It is used either in synthesizing ethylene glycols, glycol ethers, ethanolamines, and ethoxylates, or directly as a fumigant, fungicide, sterilizing, or disinfecting agent. EO is commercially obtained via selective ethylene oxidation, where the efficiency of catalysts is paramount for preventing overoxidation. Therefore, any improvements in catalyst selectivity directly translate to enormous capital savings and emission reductions.

Silver has been identified as one of the best catalyst formulations for ethylene epoxidation, and the reason has been extensively investigated. For instance, it has recently been established that the delicate structure of the silver surface and reactive oxygen, which can vary significantly among different facets in terms of activity and selectivity,[1,2] play a crucial role.[3] While the degree of oxidation of the surface in realistic operating conditions remains perplexing, studies[4–6] rule out the formation of bulk Ag_2O. Instead, an intermediate partially oxidized structure close to a phase transition is most likely responsible for the activity.[7,8]

It is foremost the ability of silver not break the C–H bonds under oxidative conditions that has allowed it to remain unrivaled as catalyst formulation despite extensive research. However, doping with antimony, bismuth, caesium, chlorine, copper, or noble metals can increase the activity and selectivity of pure silver, which is confirmed experimentally[9–16] and theoretically.[1,17–21] Substituting silver generally yields poor results because other metals tend to activate the C–H bonds. Li et al. have used scaling

[*] Dr. M. Huš, Prof. A. Hellman
Chalmers tekniska högskola, Department of Physics
Fysikgränd 3, SE-41296 Göteborg (Sweden)
E-mail: matej.hus@ki.si
anders.hellman@chalmers.se

Dr. M. Huš, Dr. M. Grilc, Dr. J. Teržan, Prof. B. Likozar
Kemijski inštitut
Hajdrihova 19, SI-1000 Ljubljana (Slovenia)

Dr. M. Huš, Dr. M. Grilc
Univerza v Novi Gorici
Vipavska 13, SI-5000 Nova Gorica (Slovenia)

Dr. M. Huš
Zveza za tehniško kulturo Slovenije
Zaloška 65, SI-1000 Ljubljana (Slovenia)

Dr. M. Huš
Zavod za varstvo kulturne dediščine
Poljanska 40, SI-1000 Ljubljana (Slovenia)

Dr. S. Gyergyek
Inštitut Jožef Stefan
Jamova 39, SI-1000 Ljubljana (Slovenia)

Prof. B. Likozar
Fakulteta za tehnologijo polimerov
Ozare 19, SI-2380 Slovenj Gradec (Slovenia)

relations to show that Ag is better than other IB metals, such as Cu and Au,[22] due to the trade-off between selectivity and partial oxidation activity. Torres showed that Cu is active for the reaction, albeit with lower selectivity,[23] while gold is not.[24] Kokalj et al. studied Ag, Au, Cu, and Rh, and confirmed that only Ag and, to a lesser extent, Cu are realistically useful for epoxidation.[25] Xu et al. performed the largest ab initio catalyst screening study for ethylene epoxidation so far, and while using a steady-state approximation for kinetic modeling, and fixed and reconstructed metal-oxide adlayers, the study indicates that some transition metals can potentially improve the catalytic selectivity of doped Ag catalysts, which they did not experimentally validate.[26] Altogether, several silver formulations have been proposed with higher selectivities.[27–30] However, these are less suitable for industrial settings because the intricate synthesis protocols cannot be easily scaled up.

Research on silver catalysts for ethylene epoxidation has been ample in the past decades, and several Ag catalysts have been synthesized and tested.[31] Several authors report high selectivities at reasonable conversions. However, these catalysts cannot be easily mass-produced and are ill-suited for large-scale industrial operations (for instance, using electrorefined Ag foil,[27] multi-step[29] and complex synthesis[30] or requiring precise nanostructures, such as rods[28]). Best performing catalysts require several promoters (Re, alkali, earth alkaline, and transition metals),[32] making their synthesis non-trivial and expensive. Other seemingly non-promoted Ag catalysts with high selectivities contain metal (such as Cu and Au) and other impurities (Na, K, As) as leftovers from the purification process.[33] Pure Ag catalysts, produced in a simple manner, generally have lower selectivites.[30]

Computational-led catalyst design has been the holy grail of catalysis and is being made possible with recent advances in computing power and theoretical concepts, such as scaling relations[34–36] and Brønsted–Evans–Polanyi (BEP) relations[37,38] and single-atom alloys models (SAA),[39,40] which have been used for computationally-led catalyst design.[41] While scaling relations and BEP relations form a solid theoretical foundation for the reduction of variables in the description of catalytic properties of different materials,[42] they are usually used for modeling individual rate-determining reactions on immutable catalyst surfaces.[26] Herein, we extend such endeavors to predicting the entire reaction pathway (including side reactions and end product decomposition) using density functional theory (DFT), full kinetic modeling (surpassing conventional simplified stationary-state or rate-determining-step approximations), and surface oxidation (oxygen adlayer formation). To systematically probe if and how we can improve existing Ag catalysts for ethylene epoxidation, we scan the entire metallic *s*, *d* and *p* blocks of the periodic table, including bimetallic and trimetallic combinations.

We identify the most promising catalyst formulations, which we then synthesize, characterize and test. We show that accounting for the effects of oxygen coverage on the reaction rates is paramount for producing correct trends, allowing us to arrive at a robust predictive model that explains the experimentally known facts (e.g., unique properties of alkali doping) and allows for the prediction of better formulations. Furthermore, we specifically include further EO decomposition on the catalyst, which explains why some catalysts fail to produce noticeable amounts of epoxide despite favourable kinetics and thermodynamics of its formation. As predicted computationally, Ag/CuCd and Ag/CuPb were experimentally confirmed as superior to Ag or Ag–Cu, while still retaining simple synthesis procedures.

Results and Discussion

Mechanistic differences

Despite being a complex reaction, ethylene epoxidation is generally characterized by two crucial steps: the formation of oxametallocycle (OMC) and its conversion to EO.[1,17–21] To be able to construct a full microkinetic model, we postulate that the reaction mechanism can be veraciously described as commencing with non-activated adsorption of C_2H_4 (Reaction 1) and O_2 (R. 2), which dissociates into two O* surface atoms (R. 3). Next, these can react with C_2H_4 to form oxametallocycle (OMC) (R. 4), which converts either into epoxide (R. 5) or acetaldehyde (R. 6). While they then desorb (R. 7 and 8), acetaldehyde rapidly and homogeneously (uncatalyzed) burns to CO_2 and H_2O, which is modeled as an instantaneous lump reaction (R. 13).

Such a model would yield erroneous predictions since the selectivity is not influenced merely by the ratio of OMC conversion reaction rates ($r_5 > r_6$). When vinylic hydrogen atoms are too reactive, no OMC is formed in the first place and ethylene undergoes rapid combustion. Therefore, we explicitly add the two most important side reactions to account for this. First, ethylene can remove its vinylic hydrogen in a non-assisted manner (R. 9) or by a helping co-adsorbed O* species (R. 10). We considered the conversion of the ensuing products into CO_2 and H_2O as a rapid, non-rate determining reaction (similarly to R. 13). Furthermore, the formed EO could decompose on the catalyst prior to desorption or upon readsorption. This decomposition is lumped into two separate reactions: non-assisted hydrogen stripping from EO (R. 11) or O*-mediated hydrogen stripping from EO (R. 12), both followed by a rapid conversion to CO_2 and H_2O. The reaction mechanism (Figure 1) is formally written in Scheme 1.

The model rests on the assumption that the same reaction network is *accessible* on all surfaces since we wish the model to be transferable and uniform, while different reactions predominate on different catalysts. As a first part of a pre-screening study for more complex alloy catalysts, this does not imply the stability of individual elements under oxidating reactive conditions nor that all elements behave similarly, which is tested later on experimentally.

A proxy for the activity of the investigated catalysts are the absolute values of the activation barriers, particularly for oxygen dissociation (R. 3). However, the selectivity is a

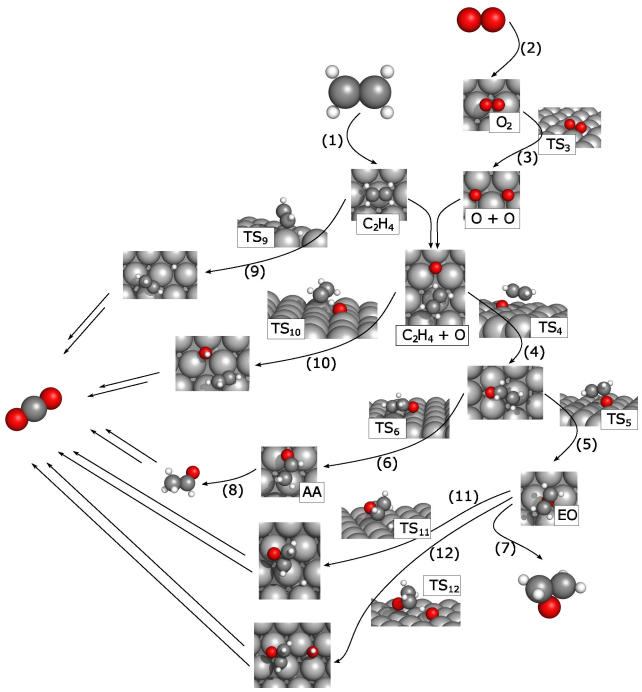

Figure 1. Scheme of the reaction mechanism on Ag(111). The reactions are numbered as in the main text. The mechanism on other investigated surfaces is analogous.

$$C_2H_4(g) + * \underset{r'_1}{\overset{r_1}{\rightleftharpoons}} C_2H_4^* \quad (1)$$

$$O_2(g) + 2* \underset{r'_2}{\overset{r_2}{\rightleftharpoons}} O_2^{**} \quad (2)$$

$$O_2^{**} \underset{r'_3}{\overset{r_3}{\rightleftharpoons}} 2\,O^* \quad (3)$$

$$C_2H_4^* + O^* \underset{r'_4}{\overset{r_4}{\rightleftharpoons}} OMC^* + * \quad (4)$$

$$OMC^* \underset{r'_5}{\overset{r_5}{\rightleftharpoons}} EO^* \quad (5)$$

$$OMC^* \underset{r'_6}{\overset{r_6}{\rightleftharpoons}} AA^* \quad (6)$$

$$EO^* \underset{r'_7}{\overset{r_7}{\rightleftharpoons}} EO(g) + * \quad (7)$$

$$AA^* \underset{r'_8}{\overset{r_8}{\rightleftharpoons}} AA(g) + * \quad (8)$$

$$C_2H_4^* + * \xrightarrow{r_9} C_2H_3^* + H^* \quad (9\dagger)$$

$$C_2H_4^* + O^* \xrightarrow{r_{10}} C_2H_3^* + OH^* \quad (10\dagger)$$

$$EO^* + * \xrightarrow{r_{11}} C_2H_3O^* + H^* \quad (11\dagger)$$

$$EO^* + O^* \xrightarrow{r_{12}} C_2H_3O^* + OH^* \quad (12\dagger)$$

$$2\,AA(g) + 5\,O_2(g) \xrightarrow{\text{fast}} 4\,CO_2(g) + 4\,H_2O(g) \quad (13)$$

Scheme 1. The universal reaction mechanism of allowed reaction on all catalysts. (†) Practically, these reactions are treated as if yielding AA, which quickly (R. 13) converts into CO_2. See Supporting Information for details.

function of the *difference* between the activation barriers for different elementary reactions.[43] For a measurable production of epoxide, the following differences must all be negative (meaning that the desired reaction has a *lower* E_A and is therefore more favorable than the alternative reactions):

$$\Delta E_{A,HS} = E_{A,4} - E_{A,10}$$

(non-assisted vinylic hydrogen stripping),

$$\Delta E_{A,OME} = E_{A,4} - E_{A,9}$$

(O-assisted hydrogen stripping),

$$\Delta E_{A,EO} = E_{A,5} - E_{A,6}$$

(formation of AA),

$$\Delta E_{A,decomp} = E_{A,7} - E_{A,11}$$

(non-assisted EO hydrogen stripping),

$$\Delta E_{A,decomp+O} = E_{A,7} - E_{A,12}$$

(O-assisted EO hydrogen stripping).

DFT calculations of the reaction mechanism for the selected noble metals (Ag, Au, Co, Cu, Ni, Pd, Pt, Rh, Ru) were performed to study the reactivity of different metals from a fundamental point, to ascertain BEP correlations as a pre-screening study for more complex alloy catalysts (see below). Four distinct scenarios are discovered, each shown in Figure 2a (for the complete list, see Supporting Information). The results show that only Ag, Au, Cu, and to some extent Pd do not activate the C–H bond of ethylene (negative $\Delta E_{A,HS}$). On these catalysts (and Rh), active O* also preferentially reacts with ethylene to OMC, while others cleave off the hydrogen atoms (negative $\Delta E_{A,OME}$). Among these, only Cu and Ag manage to convert OMC to EO in any appreciable amount (negative or slightly positive $\Delta E_{A,EO}$), as expected.[25] Both have favourable values of $\Delta E_{A,decomp}$ and $\Delta E_{A,decomp+O}$, meaning that EO is desorbed rather than decomposed provided a sufficient flux.

Interestingly, none of the nine tested catalysts decomposes EO with the help of the adsorbed atomic oxygen (barriers for R. 12 are larger than EO adsorption energy). However, non-assisted EO decomposition, which begins with hydrogen atom stripping, proceeds readily on catalysts, which are known to have a strong affinity towards hydrogen (Co, Ni, Pd, Pt, Rh and Ru). These have comparable (Co, Ni, Pd, Pt) or lower barriers (Rh and Ru) for hydrogen stripping than EO desorption.

The PESes can be easily compared among the metals and obtained for other formulations without laborious DFT simulations due to their correlation with descriptors. As shown in Figure 2b, using the adsorption strength of the carbon atom, E^C_{ads}, the oxygen atom, E^O_{ads}, or *one* linear combination ($0.7\,E^O_{ads} + 0.3\,E^C_{ads}$) thereof suffices to uniquely describe the adsorption energies, reaction energies and barriers for ethylene epoxidation on any catalyst surface.

Lastly, metals exhibit vastly different affinity towards oxygen (energetics for R. 3), which leads to a very different surface oxygen coverage,[44] which must be accounted for in a veracious model description (see below). The metals can be grouped into three classes: (*i*) Ag and Au exhibit high activation barriers for the dissociation of oxygen, which is endothermic (Au) or only slightly exothermic (Ag); (*ii*) Pd

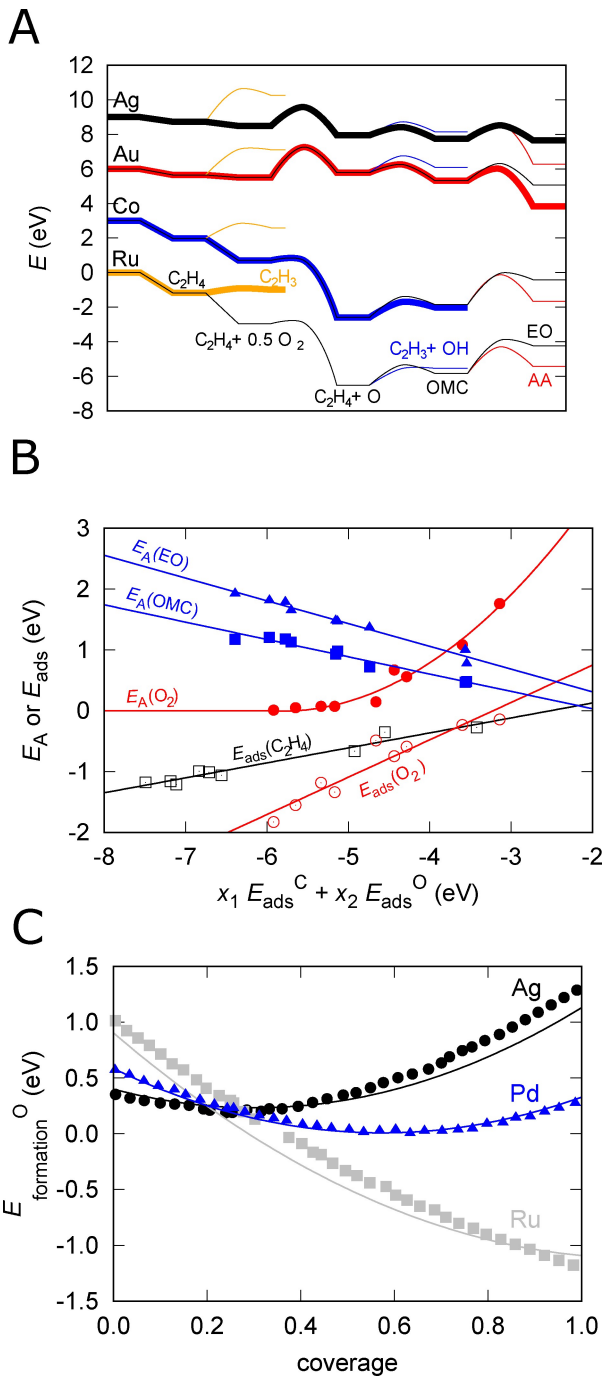

Figure 2. A) Reaction energy coordinates for different metals (Ag, Au, Co, Ru), showing four characteristic scenarios: the desired EO route (black) and the undesired AA route (red) oxygen-assisted vinylic stripping (blue), unassisted vinylic stripping (orange). The most probable pathway is shown in bold. Note that the plots are staggered for 3 eV for better legibility. B) DFT-calculated scaling relations for selected adsorption energies (empty symbols: ○ O_2; □ C_2H_4) and activation barriers (full symbols: ● O_2 dissociation; ■ OMC formation; ▲ EO formation) as a function of descriptors (E^O_{ads}, E^C_{ads}) for Ag, Au, Co, Cu, Ni, Pd, Pt, Rh, Ru. Colour code represents the descriptors used (red: $x_O=1$, $x_C=0$; black: $x_O=0$, $x_C=1$; blue: $x_O=0.7$, $x_C=0.3$). C) Formation energies for adsorbed O* as a function of coverage for three metals. Data from Frey et al.[44] Lines represent the global fit as a function of descriptors, E^O_{ads}, for the metals investigated in this work. The closely related average adsorption energies are shown in the Supporting Information.

and Pt are moderately reactive towards oxygen, (*iii*) while Co, Cu, Ni, Rh, and Ru are readily oxidized. Oxygen coverage, being negligible only for Au, noticeably changes the energetics of the reactions due to lateral interactions with oxygen adsorbates (see Supporting Information), as it has been shown several times.,[45,46] and can be assessed from DFT.[47]

Using the oxygen-oxygen lateral interaction data from Frey et al.,[44] we produced a global fit of oxygen formation energy on every metal, based solely on a value of the descriptor E^O_{ads}. As shown in Figure 2c, the complexity of oxygen interplay can be reasonably summarised into one parameter, allowing us to treat the lateral interaction between the oxygen atoms in all reaction steps where O* occurs in the mechanism. This affects the reaction energy (due to the changed energy of O*) and the reaction barriers (according to the BEP relations). The plotted formation energies represent the minimum energy hull of multiple configurations. The closely related adsorption energies, which are monotonous functions of the coverage, and their relations are shown in the Supporting Information.

Contrary to the popular screening approaches with no kinetic modelling,[48] only steady-state approximation kinetics[26] or microkinetics without side reactions,[48] we constructed a full microkinetic model of an idealized reactor with side reactions and oxygen-coverage effects, as described in the Supporting Information. For all possible descriptor values, kinetic parameters were estimated from the scaling relations correlations and cast in the full microkinetic model, allowing us to observe the production of EO as a function of time. As shown in the Supporting Information, the conversion in a model simulated reactor is predicted to be rapid. For comparing different catalyst materials, the steady state is important. The maximum turnover frequencies for the production of EO (TOF_{EO}) and the selectivity towards EO are shown as a function of the descriptors in Figure 3. They do not overlap entirely because selectivity can be depressed if high TOF_{EO} is accompanied by fast oxidation or decomposition, as well (due to Reactions 6, 9, 10, 11 and 12). However, since the narrow top of the volcano in Figure 3a lies entirely within the broader top plateau of the selectivity volcano (Figure 3b), further analysis will focus on the former.

We also note that volcanoes in Figures 3a and b are not as symmetric or regularly shaped as commonly presented in the literature[26,49,50] because of the aforementioned details of our model, such as no neglected steps and including oxygen-oxygen lateral interactions. As shown in the Supporting Information, the latter qualitatively change the predictions. We argue that this is a prerequisite for the catalyst screening aiming for a more veracious description of the catalytic reaction. Omitting it would predict an artificially increased oxygen coverage (surface approaching Ag_2O, which had been ruled out)[6] and shift the volcanoes to an area devoid of metals (see Supporting Information).

In reality (Figures 3c–d), the metals near the volcano maximum have a non-negligible oxygen coverage, ranging from 0.35 for Ag to 0.99 for In and a small but non-zero

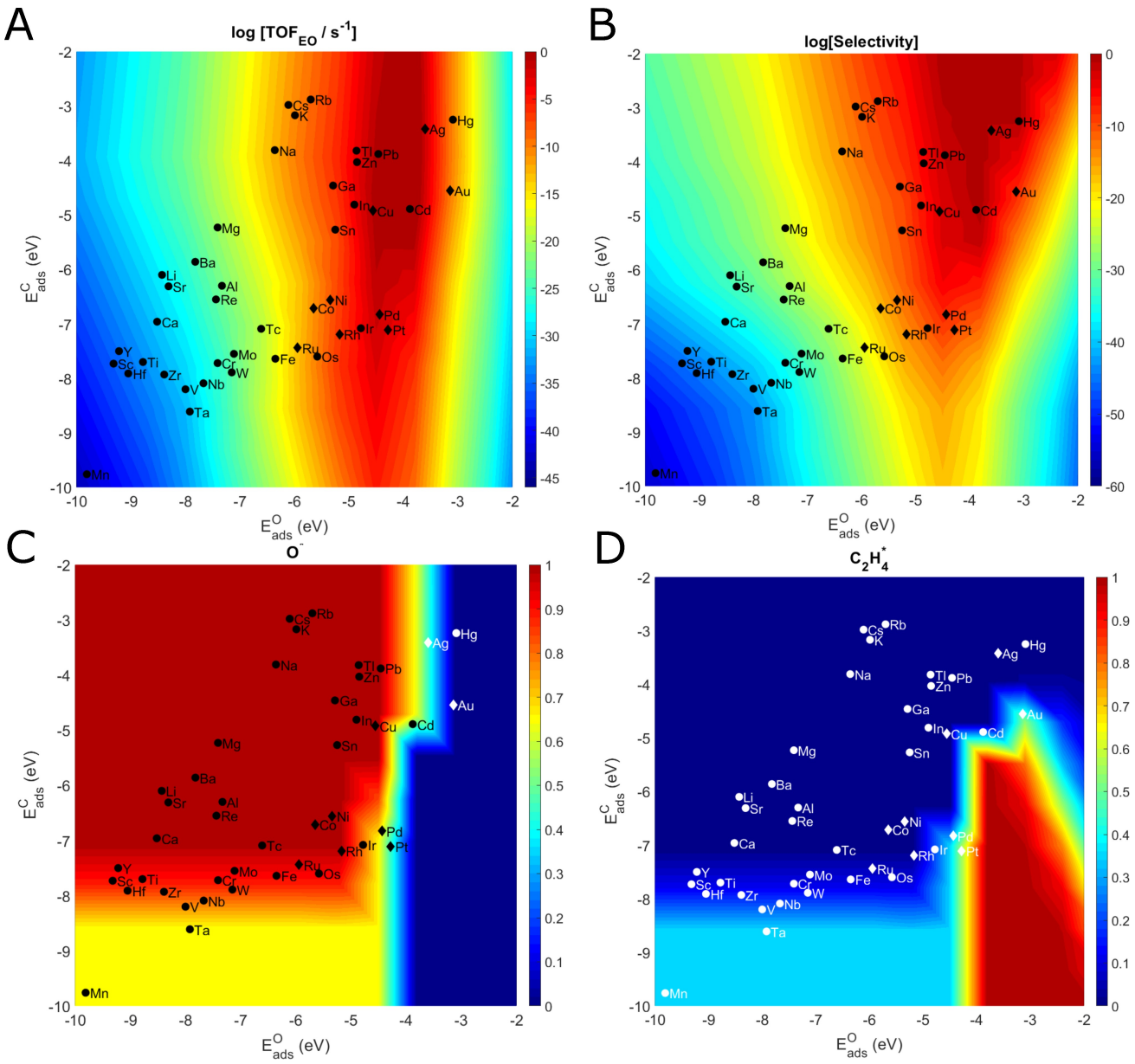

Figure 3. Volcano plot for the A) calculated turn-over frequency of EO formation and B) selectivity, and surface coverage with C) atomic oxygen (O*) and D) adsorbed ethylene (C_2H_4*) at 498 K, 0.5 bar O_2 and 0.5 bar C_2H_4 as a function of the descriptors E^O_{ads} and E^C_{ads} from a full microkinetic model. The calculated descriptors for all investigated metals are superimposed. Diamonds denote the metals used for the parametrization of the scaling relations, circles denote the metals that were only screened.

coverage (≈0.02) of ethylene (see Discussion), which warrants further discussion. While Ag_2O does not form,[51] surface reconstruction and the formation of a thin oxide layer are possible. Early STM images and simulations showed terraces of reconstructed Ag(111)-p(4×4)-O.[52] Later research has shown a coexistence of two Ag_6 triangles on the surface, interspersed by six O atoms.[53] The authors point out that while the stoichiometric surface composition equals Ag_2O, it is not similar to bulk silver oxide. Instead, it can be viewed as an arrangement of O atoms, embedded between patches of fcc- and hcp-like Ag(111).[53] A partial oxygen coverage upon reconstruction has also been considered by Xu et al. in their recent computational study.[26]

This is consistent with the predictions of our model. While the raw DFT data were harvested on extended metallic surfaces, the effects of oxygen coverages are included explicitly in the microkinetic modelling, where they impact the kinetic parameters and reaction rates. For Ag, the observed oxygen coverage hovers around 0.35, which is close to the stoichiometric coverage predicted experimentally[51,53] and accounted for computationally.[26] Furthermore, the barriers computed by Xu et al.[26] are consistent with ours (inspecting the most important quan-

tity, we observe $\Delta E_{A,EO} = 0$ eV on Ag, whereas they compute −0.01 eV).

Multi-elemental catalysts

Assuming that the descriptors of different metals in alloys are linearly additive and accepting the experimentally well-known superiority of Ag catalysts, the volcano plot (Figure 3) guides us to focus on Ag formulations with added Au, Cd, Cu, Hg, In, Pb, Tl, and Zn, which lie near the volcano maximum and have the potential to outperform Ag. To go beyond the conventional approach of solely interpreting scaling relations, we re-investigated their mechanism with full DFT on one-surface-atom substituted (3×3) supercells (Ag_8X surface composition), shown in Figure 4e (note that this does *not* imply probing an 11.1 % doped catalyst; since we position adsorbates near the dopant atoms, such a supercell is used solely to investigate single atom substitutions occurring in miscible binary alloys). In practice, dopant atoms can aggregate, bringing their catalytic activity closer to bulk material, which was probed by the monometal catalyst screening (see above).

A similar approach of using (2×2) supercells was first used by Linić et al.[54] to explain the superior performance of Ag/Cu catalysts. Mhadeshwar and Barteau used a similar approach with $Ag_{14}X$ (X = Cu, Pd, Pt, Cd, Au, Rh, ir, Zn, Ni, Os) without descriptors.[55] Ag/Pd catalysts were subsequently shown to be able to improve selectivity under a certain set of conditions.

Analyzing the DFT-computed barriers for oxygen dissociation (R. 3) and the fate of OMC ($\Delta E_{A,EO}$), Ag/Cu, Ag/Zn and Ag/Cd stand out as promising candidates (Figure 4e). Using these data and the oxygen lateral interaction (a weighted average of the descriptors for Ag and the alloyed metal in the global fit), full microkinetic

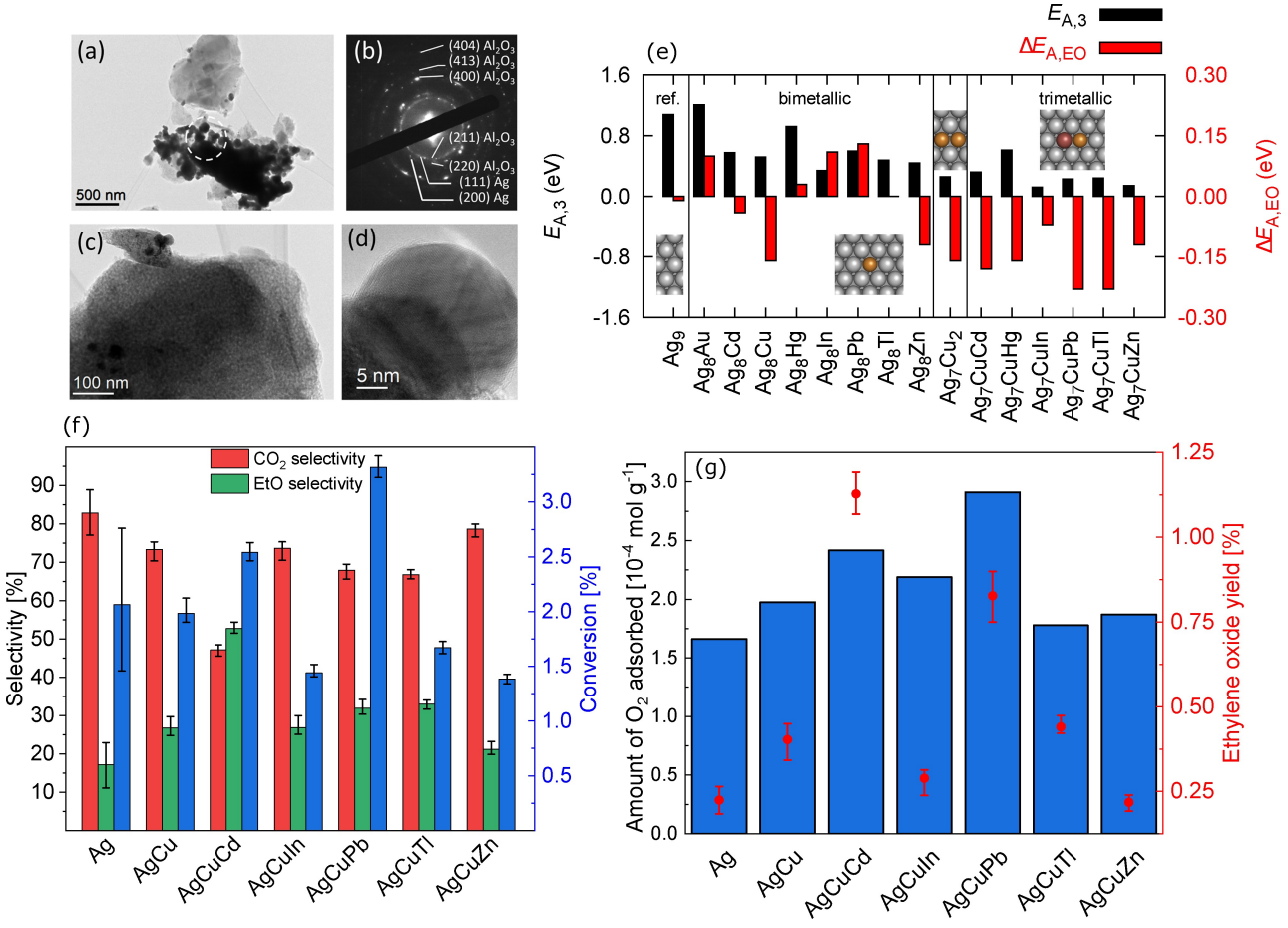

Figure 4. A) Low-magnification TEM image of Ag catalyst particles, B) selected-area electron diffraction pattern acquired from the encircled area, C) higher magnification TEM image of the Ag catalyst particle and D) high-resolution TEM image of an individual Ag nanoparticle found in Ag a catalyst particle. E) DFT-calculated properties of bimetallic and trimetallic alloys. Activation barriers for dissociative oxygen adsorption, $E_{A,3}$ (in black), describe the catalyst activity. The difference between the activation barriers for EO and AA formation, $\Delta E_{A,EO}$ in red, on one- and two-surface-atom substituted (3×3) Ag(111) supercells predict the catalyst selectivity. *Lower* (and more negative) values are advantageous for EO production. F) Ethylene conversion (blue, right axis), and the selectivity towards CO_2 (red, left axis) and ethylene epoxide (green, left axis) of the synthesized materials (50 mg of the catalytic material, mixed with 100 mg of SiC) during catalytic testing in a 6 mm quartz tube. Reaction conditions: 225 °C, 4 mL min^{-1} of ethylene and 4 mL min^{-1} of oxygen in 10 mL min^{-1}. He. G) Normalized adsorption of oxygen per gram of material (from O_2-TPD), overlaid with epoxide yield in catalyst testing.

modeling was performed at 498 K (corresponding to the experimental tests, see below), 0.5 bar O_2 and 0.5 bar C_2H_4. A good performance of Ag/Cu might be rationalized from the inspection of the volcano plot in Figure 3b, where the two metals lie very close to the top of the volcano. However, performing DFT studies on the SAA model shows that the descriptors are suitable and gives further insight beyond the resolution of the volcano. Experimentally, it is known that AgCu alloys exhibit several forms of copper oxides on the active catalyst surface,[8] while theoretical works have shown that single Cu atoms in an AgCu SAA model exhibit unique free-atom-like properties.

This opens up the possibility of further improving the Ag/Cu catalyst. We further studied six metal combinations of Ag/Cu with Cd, Hg, In, Pb, Tl, and Zn with DFT calculations of the full reaction mechanism and microkinetic modeling, describing trimetallic alloys with two-surface-atom substituted (3×3) supercells ($Ag_7Cu_1X_1$ surface composition). In essence, these are single-atom alloys (SAA)[39,40] models adapted to study dopants. Since it is well established that they do not necessarily follow conventional scaling relations,[56] DFT calculations were performed to analyse them.

Comparing the performance of $Ag_7Cu_1X_1$ with Ag_8Cu_1 could yield spurious predictions because the trends in adsorption on clusters in alloys surfaces are not monotonic.[57] To ascertain that the observed effects are due to the introduction of a third metal, the Ag_7Cu_2 surface composition was used as a benchmark and found to yield matching results to Ag_8Cu. The relevant energy barriers are shown in Figure 4e. The SAA model was chosen since we are probing Ag-based catalysts, where the concentrations of dopants are low, as shown in the experimental part.

$\Delta E_{A,EO}$ is more negative (favourable) than on Ag/Cu (−0.16 eV) for the following: −0.23 eV for Ag/CuPb and Ag/CuTl, and −0.18 eV for Ag/CuCd. The activation barrier for oxygen adsorption is comparable to that of Ag/Cu: 0.23 eV, 0.24 eV, and 0.32 eV for Ag/CuPb, Ag/CuTl, and Ag/CuCd, respectively, hinting at a similar activity (note that these values must be compared to the value of Ag_7Cu_2 (0.26 eV) and not Ag_8Cu (0.49 eV)). Ag/CuPb, Ag/CuTl, and Ag/CuCd are identified as possibly possessing superior selectivity to Ag/Cu on account of a more favorable $\Delta E_{A,EO}$ value, while they are predicted to be comparably active as Ag/Cu. In all instances, the barriers for non-assisted or O-assisted EO decomposition are larger than the desorption energies (1.7 eV and 0.8 eV vs. 0.3 eV).

Experimental validation

To ascertain the reliability of the predictive model, we synthesized the most promising catalyst formulations. As a benchmark, the pure silver catalyst was also prepared to avoid the uncertainty attached to comparing with commercial catalysts due to (undisclosed) dopants and promoters or comparability issues with literature data due to varying reaction conditions (see Discussion for literature comparison).

Experimental characterization confirmed that the catalyst particles consisted of large alumina flakes decorated with Ag nanoparticles (Figure 4a). High-resolution imaging revealed that the nanoparticles were well-crystalline, ranging from roughly 10 nm to 50 nm in size (Figure 4b). In the XRD analysis, alumina was dominant and prominent as all the peaks could be attributed to γ-Al_2O_3. The small peak of the silver phase indicated that it is in the form of nanoparticles. Using the Scherrer equation, we estimate that the average particle diameter at around 60 nm. Adding the second and third metal did not affect the mean particle diameter.

An XPS analysis of the fresh and spent catalysts showed that the bulk of the metals (silver) was in the reduced form; thus, any oxidation is limited to the surface. Doping the catalysts slightly increased their oxygen uptake (Figure 4g), as measured by in situ TPD at relevant conditions (225 °C, O_2 pulses). The trends proposed in the model agree with the chemisorption data, justifying the assumption of surface oxidation only.

In Figure 4f, we depict the averages of 5 measurements after 12 h of time on stream. This was chosen because all the catalysts underwent a stabilization period of a little over 10 h (see Supporting Information). According to the model, Ag/Cu should perform best among the bimetallic catalysts. Consistently, the experiment shows that adding minute amounts of Cu to the Ag-based catalyst increased the selectivity towards EtO (Figure 4f) and yields (Figure 4g) by more than 50 %.

The Pb- and Cu-modified catalysts exhibited the highest activity, and the highest amount of CO_2 produced. Although slightly less active, Ag/CuCd was the most selective catalyst for ethylene epoxidation, which is consistent with DFT data, where it is among the three catalysts (Ag/CuCd, Ag/CuPb, Ag/CuTl) predicted to be the most selective. The differences among them in the DFT energies are approximately 0.05 eV, which is within the accuracy of the method. Ag/CuPb performed worse, probably because it combusted a substantial amount of the formed EtO. As predicted by the model, the Ag/CuIn and Ag/CuZn are not efficient in ethylene epoxidation, underperforming even Ag/Cu. This is an important result because it proves that simply adding *any* third metal is not sufficient. The performance of Ag/CuTl deviates most from the model, which we attribute to the synthesis, where Tl could be deposited as a separate phase[58] as metallic Tl was visible on the beaker wall during synthesis. Ag/CuHg was skipped due to practical considerations and health hazard concerns.

Conclusion

The developed model, including side reactions and surface oxidation, was used to screen the periodic table for possible alternatives or additions to Ag as an epoxidation catalyst. The rough predictions from the screening were verified by DFT and validated by synthesis and catalytic tests, which

confirmed the positive effects of adding Cu/Cd and Cu/Pb to Ag.

The model epitomizes the Sabatier principle. Comparing Figures 3c and d with the experimental yields (Figure 4f), it is clear that Pb and Cd provide the greatest boost to catalytic performance since they lie in the intermediate region with significant coverages of *both* ethylene and oxygen, which is not the case for other metals. In situ oxygen chemisorption shows that doping with Cd, In, and Pb increases oxygen adsorption, while Tl and Zn decrease it, which is congruent with the model predictions (Figure 3c). This shows that increasing oxygen coverages translates to larger yields of EO up to a point, which is exceeded with Pb. Thus, while important, oxygen coverage is not the sole factor determining the EO yield.

While we focused on its predictive capabilities, the devised model has substantial descriptive power and also captures the experimentally previously observed facts, such as the beneficial effect of alkali doping, usually Cs. This has been mechanistically variously attributed to the deactivation of the acidic sites on the support (which decompose the produced EO),[59] direct interaction with Ag surface,[60] blocking unselective sites,[14] a favoured formation of electrophilic oxygen,[61] stabilization of the EO yielding transition state[20,43,62] and stabilization of the Ag surface morphology.[63] Our model shows that despite a large permissible range of E_{ads}^{C}, most metals lie below the critical value $E_{ads}^{C} = -5$, which is crucial for the selectivity (see Figure 3b). Notable exceptions are heavier alkali metals (K, Cs, Rb), of which Cs is especially known experimentally[14,64,65] and theoretically[20,43] to be a beneficial dopant. These alkali metals have particularly high E_{ads}^{C} values (and low E_{ads}^{O}), meaning they can be used to alloy the catalyst and lower its E_{ads}^{O} value without decreasing E_{ads}^{C}. On the volcano plots in Figures 3a–d, this is seen as a left-to-right movement (and even slightly upwards). Thus, the exact mode of action becomes *irrelevant* as the role of Cs is trimmed down to its favourable (less negative) value for the descriptor E_{ads}^{C}. On the other hand, strongly negative values of alkali E_{ads}^{O} values imply they must only be added in small amounts, not as co-catalysts or alloys, which is well-established experimentally.[60] Care must be taken when extrapolating from the model, where the elements in the metallic form were used for its construction. Alkalis, such as Cs, are not metallic under the reactive conditions. This is reproduced by the model itself, showing a 1 ML oxygen coverage, which corresponds to the cationic form. Similarly, Re is known to positively influence the performance of silver catalysts.[66] Nevertheless, we focused on the immediately adjacent metals to the volcano top in further investigation to avoid cherry-picking individual elements and instead maintain the model ab initio, having in mind that such a model is not exhaustive.

In our work, three goals were pursued. First, a comprehensive reaction model was developed, suitable for catalyst screening at the *atomic* scale, and several promising candidates were identified. Second, the identified catalysts had to have simple synthesis protocols (precipitation), allowing for quick and cheap mass production. Thirdly, although known to improve selectivity considerably, we intentionally avoided co-feeding chlorides, such as ethylene dichloride or ethyl chloride, for environmental and economic reasons, as well as, to reproduce modeling efforts as truthfully as possible.[62]

The synthesis precursors and protocol, experimental set-up and conditions were chosen as to amplify the *differences* and *trends* between the tested catalysts even at the expense of raw yields. High-porosity we used is known to give lower yields.[67] Yield improvements could be achieved by altering the WHSV (weight hourly space velocity), C_2H_4:O_2 ratio, feed flow, the size of the reactor hot zone, the catalyst synthesis protocol (changing the support and/or Ag:dopant ratio) or reactor design (such as membrane reactor). Nevertheless, Ag/CuPb and Ag/CuCd, produced in an easy-to-scale-up process, showed comparable yields to much more refined catalysts, all while being identified by first-principles exclusively.

Thus, the model successfully bridges the gap between the two extremes: ab initio theoretical simulations and industrial applicability. It has been shown to possess the complexity required to describe experimental data and produce testable predictions, yet it remains computationally feasible. Moreover, the calculated descriptors and surface oxidation properties allow for its generalization to other industrially important reactions, such as the (reverse) water-gas shift reaction, ammonia synthesis, and many others.

Computational resources

The computer time was provided by the Swedish National Infrastructure for Computing (SNIC) at C3SE (Gothenburg) and NSC (Linköping), and by the National Institute of Chemistry in Slovenia (Ljubljana) and HPC RIVR consortium and EuroHPC JU through HPC system Vega at the Institute of Information Science, Maribor, Slovenia.

Author contributions

This work represents the collaborative efforts of all the authors involved. M.H. and A.H. conceptualized the study and wrote the paper. M.H. and M.G. performed the computations. J.T. synthesized the catalysts and tested them, and wrote the experimental part of the paper. J.T. and S.G. performed catalyst characterisation. B.L. and A.H. provided counsel and acquired funding. M.H. and A.H. finalised the paper.

Acknowledgements

This research was supported by the Slovenian Research Agency (core funding P2-0152, infrastructure funding I0-0039 and project funding N1-0303, J2-4424). S.G. appreciates the core funding P2-0089 from the Slovenian Research Agency. M.H. and A.H. are also grateful for the financial

support by the Knut and Alice Wallenberg Foundation (Project 2015.0057) and the Swedish Research Council (Project 2015-03773). We thank Dr. Mikkel Jørgensen and Dr. Adam Arvidsson for indispensable discussions, and Dr. Ana Kroflič for endless inspiration.

Conflict of Interest

The authors have no conflicts to declare.

Data Availability Statement

The data that support the findings of this study are available in the Supporting Information of this article.

Keywords: Catalyst Screening · DFT · Ethylene Epoxidation · Experimental Validation · Modelling

[1] P. Christopher, S. Linić, *J. Am. Chem. Soc.* **2008**, *130*, 11264.
[2] M. Huš, A. Hellman, *ACS Catal.* **2019**, *9*, 1183.
[3] T. E. Jones, T. C. R. Rocha, A. Knop-Gericke, C. Stampfl, R. Schlögl, S. Piccinin, *ACS Catal.* **2015**, *5*, 5846.
[4] G. Rovida, F. Pratesi, M. Maglietta, E. Ferroni, *J. Vac. Sci. Technol.* **1972**, *9*, 796.
[5] A. Michaelides, K. Reuter, M. Scheffler, *J. Vac. Sci. Technol. A* **2005**, *23*, 1487.
[6] N. M. Martin, S. Klacar, H. Grönbeck, J. Knudsen, J. Schnadt, S. Blomberg, J. Gustafson, E. Lundgren, *J. Phys. Chem. C* **2014**, *118*, 15324.
[7] M. T. Greiner, T. E. Jones, A. Klyushin, A. Knop-Gericke, R. Schlögl, *J. Am. Chem. Soc.* **2017**, *139*, 11825, pMID: 28753282.
[8] M. T. Greiner, J. Cao, T. E. Jones, S. Beeg, K. Skorupska, E. A. Carbonio, H. Sezen, M. Amati, L. Gregoratti, M.-G. Willinger, A. Knop-Gericke, R. Schlögl, *ACS Catal.* **2018**, *8*, 2286.
[9] C. T. Campbell, M. T. Paffett, *Appl. Surf. Sci.* **1984**, *19*, 28.
[10] C. T. Campbell, B. E. Koel, *J. Catal.* **1985**, *92*, 272.
[11] C. T. Campbell, *J. Catal.* **1986**, *99*, 28.
[12] J. T. Jankowiak, M. A. Barteau, *J. Catal.* **2005**, *236*, 366.
[13] J. T. Jankowiak, M. A. Barteau, *J. Catal.* **2005**, *236*, 379.
[14] M. Atkins, J. Couves, M. Hague, B. Sakakini, K. Waugh, *J. Catal.* **2005**, *235*, 103.
[15] K. Waugh, M. Hague, *Catal. Today* **2010**, *157*, 44.
[16] T. C. Rocha, M. Hävecker, A. Knop-Gericke, R. Schlögl, *J. Catal.* **2014**, *312*, 12.
[17] S. Linić, M. A. Barteau, *J. Am. Chem. Soc.* **2002**, *124*, 310.
[18] S. Linić, M. A. Barteau, *J. Am. Chem. Soc.* **2003**, *125*, 4034.
[19] S. Linić, M. A. Barteau, *J. Catal.* **2003**, *214*, 200.
[20] S. Linić, M. A. Barteau, *J. Am. Chem. Soc.* **2004**, *126*, 8086.
[21] A. C. Lukaski, M. A. Barteau, *Catal. Lett.* **2009**, *128*, 9.
[22] H. Li, A. Cao, J. K. Nørskov, *ACS Catal.* **2021**, *11*, 12052.
[23] D. Torres, N. Lopez, F. Illas, R. M. Lambert, *J. Am. Chem. Soc.* **2005**, *127*, 10774.
[24] D. Torres, F. Illas, *J. Phys. Chem. B* **2006**, *110*, 13310, pMID: 16821848.
[25] A. Kokalj, P. Gava, S. de Gironcoli, S. Baroni, *J. Catal.* **2008**, *254*, 304.
[26] H. Xu, L. Zhu, Y. Nan, Y. Xie, D. Cheng, *ACS Catal.* **2021**, *11*, 3371.
[27] D. Jingfa, Y. Jun, Z. Shi, Y. Xiaohong, *J. Catal.* **1992**, *138*, 395.
[28] P. Christopher, S. Linic, *ChemCatChem* **2010**, *2*, 78.
[29] K. R. Iyer, A. Bhan, *ACS Catal.* **2021**, *11*, 14864.
[30] B. T. Egelske, W. Xiong, H. Zhou, J. R. Monnier, *J. Catal.* **2022**, *410*, 221.
[31] T. Pu, H. Tian, M. E. Ford, S. Rangarajan, I. E. Wachs, *ACS Catal.* **2019**, *9*, 10727.
[32] "Process for Initiating a Highly Selective Ethylene Oxide Catalyst": N. Rizkalla, N. B. Castagnola, Girish Desai (Scientific Design Co. Inc.), US8487123B2 2**013**.
[33] T. Pu, A. Setiawan, B. Mosevitzky Lis, M. Zhu, M. E. Ford, S. Rangarajan, I. E. Wachs, *ACS Catal.* **2022**, *12*, 4375.
[34] V. Pallassana, M. Neurock, *J. Catal.* **2000**, *191*, 301.
[35] J. Nørskov, T. Bligaard, A. Logadottir, S. Bahn, L. Hansen, M. Bollinger, H. Bengaard, B. Hammer, Ž. Šljivančanin, M. Mavrikakis, Y. Xu, S. Dahl, C. Jacobsen, *J. Catal.* **2002**, *209*, 275.
[36] F. Abild-Pedersen, J. Greeley, F. Studt, J. Rossmeisl, T. R. Munter, P. G. Moses, E. Skúlason, T. Bligaard, J. K. Nørskov, *Phys. Rev. Lett.* **2007**, *99*, 016105.
[37] S. Trasatti, *J. Electroanal. Chem. Interfacial Electrochem.* **1972**, *39*, 163.
[38] A. J. Medford, A. Vojvodic, J. S. Hummelshøj, J. Voss, F. Abild-Pedersen, F. Studt, T. Bligaard, A. Nilsson, J. K. Nørskov, *J. Catal.* **2015**, *328*, 36; Special Issue: The Impact of Haldor Topsøe on Catalysis.
[39] R. T. Hannagan, G. Giannakakis, M. Flytzani-Stephanopoulos, E. C. H. Sykes, *Chem. Rev.* **2020**, *120*, 12044.
[40] R. Réocreux, M. Stamatakis, *Acc. Chem. Res.* **2022**, *55*, 87.
[41] R. T. Hannagan, G. Giannakakis, R. Réocreux, J. Schumann, J. Finzel, Y. Wang, A. Michaelides, P. Deshlahra, P. Christopher, M. Flytzani-Stephanopoulos, M. Stamatakis, E. C. H. Sykes, *Science* **2021**, *372*, 1444.
[42] H. Toulhoat, P. Raybaud, S. Kasztelan, G. Kresse, J. Hafner, *Catal. Today* **1999**, *50*, 629.
[43] M. Huš, A. Hellman, *J. Catal.* **2018**, *363*, 18.
[44] K. Frey, D. J. Schmidt, C. Wolverton, W. F. Schneider, *Catal. Sci. Technol.* **2014**, *4*, 4356.
[45] M. Stamatakis, D. G. Vlachos, *ACS Catal.* **2012**, *2*, 2648.
[46] S. Wang, V. Vorotnikov, D. G. Vlachos, *ACS Catal.* **2015**, *5*, 104.
[47] E. Hansen, M. Neurock, *Surf. Sci.* **1999**, *441*, 410.
[48] L. Xu, E. E. Stangland, M. Mavrikakis, *J. Catal.* **2018**, *362*, 18.
[49] C. H. Christensen, J. K. Nørskov, *J. Chem. Phys.* **2008**, *128*, 182503.
[50] Z.-F. Huang, J. Wang, Y. Peng, C.-Y. Jung, A. Fisher, X. Wang, *Adv. Energy Mater.* **2017**, *7*, 1700544.
[51] M. Schmid, A. Reicho, A. Stierle, I. Costina, J. Klikovits, P. Kostelnik, O. Dubay, G. Kresse, J. Gustafson, E. Lundgren, J. N. Andersen, H. Dosch, P. Varga, *Phys. Rev. Lett.* **2006**, *96*, 146102.
[52] C. I. Carlisle, D. A. King, M.-L. Bocquet, J. Cerdá, P. Sautet, *Phys. Rev. Lett.* **2000**, *84*, 3899.
[53] J. Schnadt, A. Michaelides, J. Knudsen, R. T. Vang, K. Reuter, E. Lægsgaard, M. Scheffler, F. Besenbacher, *Phys. Rev. Lett.* **2006**, *96*, 146101.
[54] S. Linic, J. Jankowiak, M. A. Barteau, *J. Catal.* **2004**, *224*, 489.
[55] A. B. Mhadeshwar, M. A. Barteau, *Mechanism in Homogeneous and Heterogeneous Epoxidation Catalysis*, Elsevier, Amsterdam, **2008**, p. 265.
[56] H. Thirumalai, J. R. Kitchin, *Top. Catal.* **2018**, *61*, 462.
[57] A. P. Monasterial, C. A. Hinderks, S. Viriyavaree, M. M. Montemore, *J. Chem. Phys.* **2020**, *153*, 111102.
[58] J. C. Dellamorte, J. Lauterbach, M. A. Barteau, *Ind. Eng. Chem. Res.* **2009**, *48*, 5943.
[59] W. S. Epling, G. B. Hoflund, D. M. Minahan, *J. Catal.* **1997**, *171*, 490.
[60] R. B. Grant, R. M. Lambert, *Langmuir* **1985**, *1*, 29.

[61] M. C. N. Amorim de Carvalho, F. B. Passos, M. Schmal, *J. Catal.* **2007**, *248*, 124.
[62] S. Goncharova, E. Paukshtis, B. Bal'zhinimaev, *Appl. Catal. A* **1995**, *126*, 67.
[63] J. Couves, M. Atkins, M. Hague, B. H. Sakakini, K. C. Waugh, *Catal. Lett.* **2005**, *99*, 45.
[64] D. S. Afanasev, N. I. Kuznetsova, V. I. Zaikovskii, *React. Kinet. Mech. Catal.* **2012**, *106*, 193.
[65] J. Teržan, P. Djinović, J. Zavašnik, I. Arčon, G. Žerjav, M. Spreitzer, A. Pintar, *Appl. Catal. B* **2018**, *237*, 214.
[66] J. C. Dellamorte, J. Lauterbach, M. A. Barteau, *Catal. Today* **2007**, *120*, 182.
[67] J. van den Reijen, W. Versluis, S. Kanungo, M. d'Angelo, K. de Jong, P. de Jongh, *Catal. Today* **2019**, *338*, 31, multiscale Catalysis.

Manuscript received: April 25, 2023
Accepted manuscript online: May 25, 2023
Version of record online: ■■, ■■

Research Articles

Heterogeneous Catalysis

M. Huš,* M. Grilc, J. Teržan, S. Gyergyek, B. Likozar, A. Hellman* —— **e202305804**

Going Beyond Silver in Ethylene Epoxidation with First-Principles Catalyst Screening

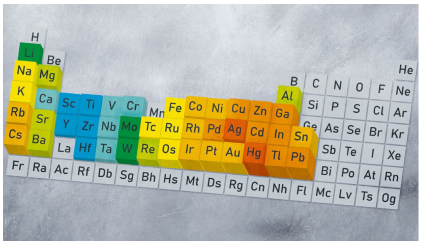

Using computational screening of the periodic table for ethylene epoxidation catalysts, Ag/CuPb, Ag/CuCd, and Ag/CuTl were identified as superior catalysts. The inclusion of surface oxidation, side reactions and epoxide decomposition is shown to be paramount to avoid erroneous predictions. The predicted catalysts were synthesised, characterised and tested, confirming the predictions.